Rapid Push Pull Resonant Charger for High Power, High Voltage Applications Using Low Input Voltage

Eyal Rotman
Department of Power Electronics
Rafael Advanced Defense Systems LTD.
P.O.Box 2250, Haifa31021, Israel
eyalrot@rafael.co.il

Shmuel (Sam) Ben-Yaakov, Fellow, IEEE
Power Electronics Laboratory
Department of Electrical and Computer Engineering
Ben-Gurion University of the Negev
P.O.Box 653, Beer-Sheva 84105, Israel
sby@ee.bgu.ac.il; Website: www.ee.bgu.ac.il/~pel

***Abstract*— This paper presents a novel approach to rapid, high power, high voltage capacitor charger that is fed from low voltage input source and achieves high efficiency in small dimensions. The charger is based on parallel resonant push-pull topology. Output current of the proposed charger is shown to be approximately constant regardless of the rising output voltage. The charged capacitor is fed by a linearly rising power profile. The behavior differs from series resonant and flyback charger topologies where output capacitor is fed by linearly decaying and constant power, respectively. The parallel resonant topology enables charging from a low voltage source using a relatively low transformer winding ratio, in one stage. The proposed charger is controlled by the digital controller dsPIC33FJ16GS502 (Microchip USA). Zero current soft switching is performed using a varying switching frequency based on continuous controller calculations during charging. Feasibility of the proposed charger and its control were tested experimentally on a prototype charger, which was operated at 0.7kW from a low input voltage source of 28V. The charger was loaded by an output capacitor of 250nF, which was charged at the rate of 600 charging cycles per second to 3kV. Good agreement was found between the proposed analytical model and experimental results.**

I. INTRODUCTION

Capacitor chargers are used in key applications in both commercial and military industries [1-2]. The main objective of capacitor chargers is to periodically operate pulsed power systems. Once the energy is transferred from the storage capacitor to the pulsed load, the capacitor needs to be recharged fast enough to meet the system repetition rate. Prominent applications include pulsed lasers, arc lamps and plasma formation. Capacitor charges are required to inject a given amount of energy to a load capacitor at a given charging time (J/sec). In contrast to standard DC-DC converters, capacitor chargers have to maintain high efficiency at a wide range of output voltages. The preferred method to transfer energy to a capacitor is by a charger that behaves as a current source. This will ease the control since a voltage source charger will require tight current feedback to avoid current spikes.

Two general topologies were proposed in the literature for capacitor charging: flyback charger [3-4] and resonant chargers [5-10]. Flyback topology operated at a constant switching frequency feeds constant power to the charged capacitor, see Figure 1. As hard switching is involved, flyback topology suits low and medium power demands even though efficiency can be improved using sophisticated snubbers [4]. The charging speed is deteriorated with rising output voltage, since transformer capacitance has to be charged to output voltage level before the output capacitor can be charged.

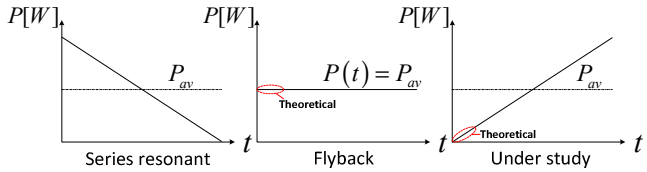

Figure 1: Charging profiles of three possible topologies.

High efficiency, high power chargers, promote the use of soft switching resonant operation. The series topology, which is the most prevalent one in publications, is characterized by a decaying average load current as the high voltage develops [5]. Figure 1 shows that higher output current must be developed at the initial charging phase in order to maintain the required average output power (J/sec), and therefore degrading efficiency. This paper shows that in the proposed topology, based on parallel resonant topology [6-7], injected charging power to output capacitor is linearly increasing, as shown in Figure 1.

The three topologies are qualitatively compared in Figure 1, assuming equal output and input voltages, with the same average charging power P_{av}. It can be seen that series topology is bounded and cannot charge to a higher voltage than it was designed for. Furthermore, charging to lower voltages result in reduced efficiency since charging is based on high currents [8]. In contrast, the proposed topology has the ability to perform efficient charging, in a wide range of output voltages. Charging currents are reduced as output

voltage is reduced. There is no upper voltage limit except power loss.

Receiving high output voltage from a low input voltage is achieved based on multiplying two different gains in resonant topologies: resonant tank gain (3) and transformer winding ratio. Series resonant topology has a resonant gain below unity and therefore achieving high output voltage is based solely on transformer winding ratio. For applications using low input voltage this results in increased transformer size because of the high transformer ratio. Parallel topology has a resonant gain above unity and therefore reduced transformer dimensions.

High power chargers, fed from low input voltage, have relatively high input current. Series and series-parallel [9] resonant topologies have difficulty handling the high currents drawn from the low input voltage source due to the very low ESR needed at the series capacitor. However, drifting of magnetization current is blocked. Common phenomenon at resonant parallel topology is an uncontrolled magnetization current [10], which could lead to transformer saturation, due to the lack of series capacitor.

The aim of this study is to investigate the proposed charger based on resonant parallel topology, develop its control and the additional technologies that enable its implementation.

II. Proposed Topology

Figure 2. The power stage includes two power switches sw_1, sw_2, power transformer T_1 with winding ratio of 1:n, resonant inductance L_r and resonant capacitor C_r. The voltage doubler at the output is comprised of capacitive load C_{out1}, C_{out2}, and two diodes D_{o1}, D_{o2}.

The resonant capacitor at the secondary transformer side and the series parasitic leakage L_r inductance form a resonant tank. The required resonant series inductance is achieved by reducing the secondary and primary coupling [11]. The doubler configuration reduces the required transformer ratio and resonant tank gain. It will be shown that reducing resonant gain reduces rms current, resulting in higher efficiency.

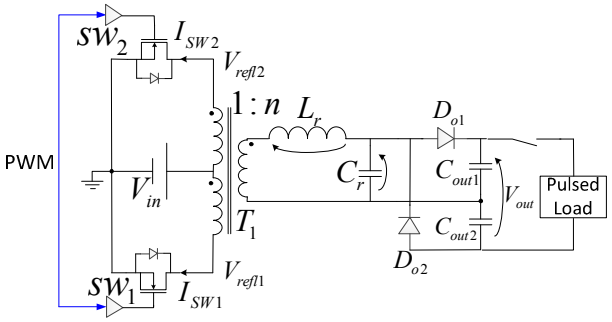

Figure 2: Charger topology under study.

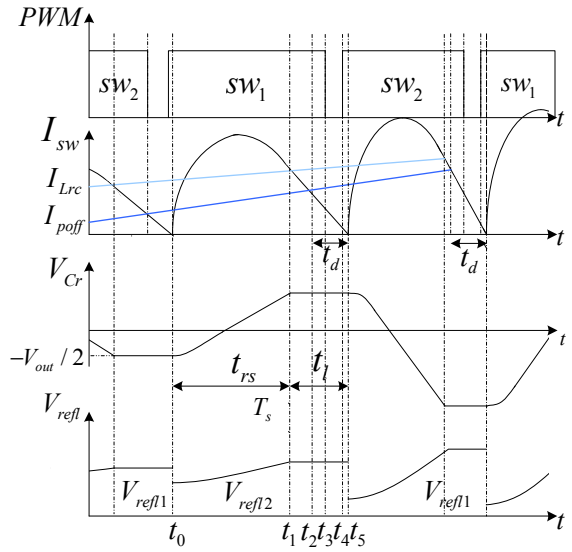

Figure 3: Key waveforms of the proposed topology. Upper trace: controller output PWM; Second trace: switches controlled current; Third trace: resonant capacitor voltage; Lower trace: reflected switch drain voltage.

The key waveforms are presented in Figure 3. Switching cycle begins at t_0 when sw_1 for example, is turned on. Switch current is increased due to the resonant between L_r, C_r, and energy is transferred from input source V_{in} to resonant inductance L_r. When C_r is recharged to $V_{out}/2$ at t_1, diode D_{o1} starts to conduct so that the voltage across C_r is clamped to that of C_{out1}.

The current decreases linearly since the negative voltage on the resonant inductor V_{Lr} is constant and energy is transferred to C_{out1}. The controller senses the switches current in order to detect threshold I_{poff}, which triggers switch turn off. Constant delay t_d from t_2 to t_5 has to be considered, taking into account software delay up to t_3, and hardware delay up to t_5, while frequency and switch current change during charging. I_{poff} threshold is calculated by the controller by sensing the output voltage in order to turn off the switches at zero current. At t_4, sw_2 is turned on causing a negligible negative dead time. During sw_1 conduction, a reflected voltage V_{refl2} appears on sw_2, determining its voltage stress. Switching cycle, T_s, is defined as the conduction time of each one of the switches. The switching cycle is composed of resonant oscillation at the first phase $t_{rs}=t_1-t_0$ and of linear decaying current at the second phase $t_l=t_5-t_1$.

III. Analytical Modeling

Analytical modeling defines the equations linking charger parameters n, Z_0, ω and charger requirements; namely, charging output capacitance C_{out} to required output voltage V_{out} at a charging time t_{ch} from a voltage source V_{in}.

Figure 4 exhibits the equivalent circuit for conduction through both switches, thus enabling to find resonant inductor current and resonant capacitance voltage, by

reflecting the power stage to transformer secondary side. Figure 4 shows polarity of resonant components while sw_1 is conducting. While sw_2 conducts the polarity is opposite.

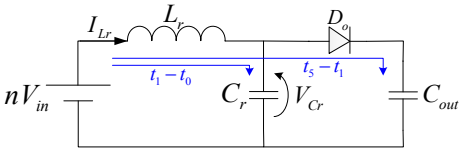

Figure 4: Equivalent power stage circuit at the conduction of sw1.

A. *Time period t_1-t_0 (resonant phase)*

During resonant phase no energy is injected to output capacitors and only reactive energy circulates at power stage. The resonance behavior between Lr and Cr is shown using normalized output voltage u, at (1),(2). $\omega = 1/\sqrt{L_r C_r}$ defines the natural frequency of the resonant tank. Initial conditions are $V_{cr}(t_0) = -V_{out}/2$ and $I_{Lr}(t_0) = 0$.

$$V_{Cr}(t) = nV_{in}\left(-u + 2(1+u)\sin^2\left(\frac{\omega}{2}t\right)\right) \quad (1)$$

$$I_{Lr}(t) = \frac{nV_{in}}{Z_0}(1+u)\sin(\omega t) \quad (2)$$

Normalized charger output voltage is defined by Eq (3). Notice that u has a dynamic behavior since output voltage is continuously changing during charging.

$$u(t) = \frac{V_{out}(t)/2}{nV_{in}} \quad (3)$$

The resonant stage is completed when diode D_o starts to conduct at t_1. At that moment the voltage across C_r is $V_{out}/2$ (when sw1 conducts). Accordingly, Eq (1) yields the resonant duration, t_{rs}:

$$t_{rs} = t_1 - t_0 = \frac{1}{\omega}\text{acos}\left(\frac{1-u}{1+u}\right) \quad (4)$$

The current value in the resonant inductance at the end of the resonant stage is:

$$I_{Lrc} = \frac{2nV_{in}\sqrt{u}}{Z_0} \quad (5)$$

where $Z_0 = \sqrt{L_r/C_r}$ is the resonant tank impedance as reflected to transformer secondary side.

B. *Time period t_5-t_1 (linear phase)*

During the linear phase, energy is injected to output capacitors. As diode D_o opens for conduction, C_{out} is loaded in parallel to the resonant capacitor. Having $C_{out} >> C_r$ the voltage dictated on L_r is practically constant and is equal to nV_{in}-$V_{out}/2$, causing the inductance current to decrease linearly. Knowing the initial current, I_{Lrc} , and the linear decaying current, we can calculate the discharge time t_l:

$$t_l = t_5 - t_1 = \frac{2}{\omega}\frac{\sqrt{u}}{u-1} \quad (6)$$

An examination of (6) shows that increasing u decreases the linear phase in which energy is injected to output capacitance. Adding expressions (4),(6) provides switching cycle T_s. Eq (7) defines the normalized switching frequency, where $\omega_s = 2\pi/2T_s$:

$$\frac{\omega_s}{\omega} = \frac{\pi}{\text{acos}\left(\frac{1-u}{1+u}\right) + \frac{2\sqrt{u}}{u-1}} \quad (7)$$

Switching frequency ω_s asymptotically converges, with increasing u , to the natural frequency of the resonant tank ω. For u>5 we can assume $\omega_s \approx \omega$ as ω_s only changes by 8%.

The amount of charge injected to load capacitor during a switching cycle, ΔQ_{out}, can be determined by integrating the resonant inductor current during the linear phase:

$$\Delta Q_{out} = 2C_r nV_{in}\frac{u}{u-1} \quad (8)$$

C. *Dynamic behavior of normalized output voltage*

The amount of energy being transferred in a switching cycle to the output capacitor is found using $\Delta E_{out} = \Delta Q_{out} V_{out}/2$:

$$\frac{\Delta E_{out}(t)}{T_s(t)} = \frac{2C_r(nV_{in})^2\frac{u^2}{u-1}}{\frac{1}{\omega}\text{acos}\left(\frac{1-u}{1+u}\right) + \frac{2}{\omega}\frac{\sqrt{u}}{u-1}} \quad (9)$$

Even though the topology under study is meant for very rapid chargers, we can still assume $T_s << t_{ch}$. Hence, $\frac{\Delta E_{out}}{T_s} \to \frac{dE_{out}}{dt}$. In addition, using $u = \sqrt{\frac{2E_{out}}{C_{out}}}/2nV_{in}$ we find the differential expression for *du*, therefore:

$$\frac{du}{dt} = \frac{1}{2Z_0 C_{out}}\frac{1}{\left(1-\frac{1}{u}\right)\text{acos}\left(\frac{1-u}{1+u}\right) + \frac{2}{\sqrt{u}}} \quad (10)$$

This differential equation shows the dynamic behavior of the normalized output voltage. Eq (10) can be integrated during charging, at time and normalized output voltage variables, at domains $[0, t_{ch}]$ and $u \in [k_0, k]$ respectively. Charging time expression is shown in (11). ZCS, at the topology under study, can only occur when $V_{out}/2 > nV_{in}$ therefore at $k_0 > 1$. k_0,k are defined at (12). V_{out} is the required output voltage of the charger.

$$t_{ch} = 2Z_0 C_{out} f_k \quad (11)$$

where $f_k \equiv \int_{k_0}^{k}\left[\left(1-\frac{1}{u}\right)\arccos\left(\frac{1-u}{1+u}\right) + \frac{2}{\sqrt{u}}\right]du$.

$$k_0 = \frac{V_{out0}/2}{nV_{in}}, \quad k = \frac{V_{out}/2}{nV_{in}} \quad (12)$$

Expression (11) shows that once the required V_{in}, V_{out}, C_{out}, are determined, charging time is influenced by two parameters only: transformer winding ratio *n* and resonant tank impedance Z_0.

D. Power stage currents during charging

Average load current, $I_{out,av}$, is the total charge injected to either one of the output capacitors at a switching cycle T_s. Equations (7), (8) enable finding the average output current:

$$I_{out,av} = \frac{\Delta Q_{out}}{T_s} = \frac{nV_{in}}{Z_0} \frac{2u}{(u-1)a\cos\left(\frac{1-u}{1+u}\right)+2\sqrt{u}} \qquad (13)$$

Using Eq (11),(12) we can evaluate the coefficient nV_{in}/Z_0 as follows:

$$\frac{nV_{in}}{Z_0} = \frac{P_{out,av}}{V_{out}/2} \cdot \frac{f_k}{k} \qquad (14)$$

where $P_{out,av} = 1/2 C_{out} V_{out}^2 / t_{ch}$.

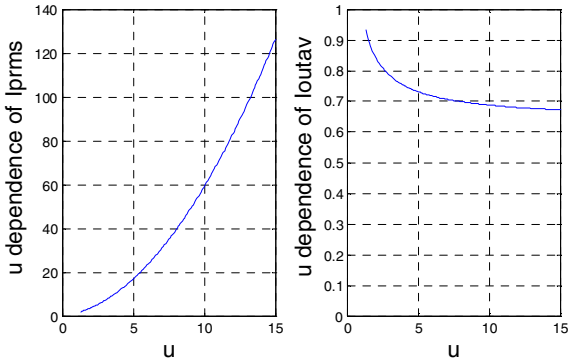

Figure 5: Normalized currents drawing. Right plot: normalized avarge load current; Left plot: normalized switches rms current. u□[k_0,k]=[1.3,15].

Rewriting Eq (13) using (14) in a normalized form provides:

$$\frac{I_{out,av}(k,u)}{\frac{P_{out,av}}{V_{out}/2} \cdot \frac{f_k}{k}} = \frac{2u}{(u-1)a\cos\left(\frac{1-u}{1+u}\right)+2\sqrt{u}} \qquad (15)$$

Examination of the left plot in Figure 5 shows the behavior of the average output current. As *u* increases during charging $I_{out,av}$ is practically stabilizing at a constant value. Above u=5, average current changes are only 8%.

The charger topology under study behaves as a current source to the output capacitor that stabilizes at a constant current value as output voltage rises, see Figure 6. Power injected to output capacitor rises approximately linearly during charging.

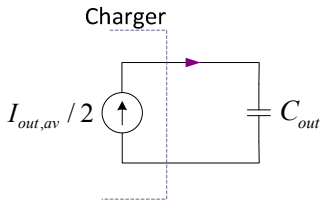

Figure 6: Equivalent charger behavior.

Using Eqs (2),(7),(14) we find the transformer secondary rms current. Reflecting it to primary winding, we obtain switches rms current, which is the main factor influencing charger efficiency.

$$\frac{I_{p,rms}(k,u)}{\frac{P_{out,av}}{V_{in}} \cdot \frac{f_k}{k^2}} = \sqrt{\frac{1}{2}(1+u)^2 - \frac{4/3u\sqrt{u}}{(u-1)a\cos\left(\frac{1-u}{1+u}\right)+2\sqrt{u}}} \qquad (16)$$

Examination of the right plot in Figure 5 shows that rms current increases rapidly through charging, while output current remains approximately constant. The different behavior of the two currents is the key for optimization of charger efficiency.

Eqs (15),(16) indicate that the developed currents are a function transformer winding ratio n and resonant tank impedance Z_0 only.

E. Magnetization voltage-sec effort

Finding transformer volt-sec magnetization inductance effort is an essential step in reducing transformer size. Having leakage inductance as resonant inductance makes this task complex since volt-sec effort depends on distributed leakage inductance between primary, xL_r, and secondary windings, $(1-x)L_r$, Figure 7. Leakage distribution ratio marked as x was found experimentally via measuring voltage reflected at the non-conducting primary winding.

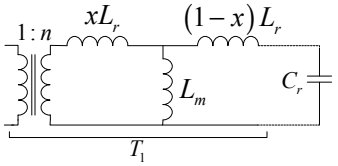

Figure 7: Leakage inductance distribution between primary and secondary windings.

Figure 7 exhibits magnetization voltage during sw1 conduction and is given in (17). Magnetization voltage is symmetrical on conjugant switching cycles. Integrating magnetization voltage during switching cycle, results in volt-sec effort expressed in (18):

$$V_{Lm}(t) = \begin{cases} nV_{in}\left(1-x\left(1+u\right)\cos\omega t\right) & 0 < t < t_{rs} \\ nV_{in}\left(1+x\left(u-1\right)\right) & t_{rs} < t < t_{rs}+t_l \end{cases} \qquad (17)$$

$$\int V_{Lm}(t)\,dt = \begin{cases} \frac{\pi n V_{in}}{\omega_s} & ,u < 1-1/x \\ \frac{\pi n V_{in}}{\omega_s} + \frac{nV_{in}}{\omega}\left(-2\arccos\frac{1/x}{1+u} + \sqrt{u^2+2u+1-1/x^2}\right) & ,u > 1-1/x \end{cases} \qquad (18)$$

The volt-sec effort is shown in Figure 8. It is shown that with increasing normalized output voltage, the effort grows linearly. This behavior is intuitive: it was shown that switching frequency converges to constant value of ω, and transformer winding voltages grow during charging. Reducing volt-sec effort is achieved by increasing resonant tank frequency while core power dissipation remains constant, as shown below.

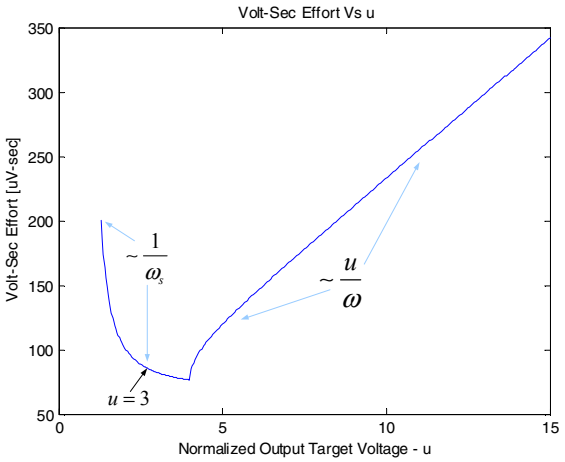

Figure 8: Prototype Volt-sec effort during charging where u∈[k0,k]=[1.3,15].

IV. Design Optomization Criteria

Finding charger optimal parameters, n,Z_0,ω is based on two optimization criteria: maximizing charger efficiency and reducing transformer dimensions.

A. Optimization criterion for maximizing efficiency

Maximizing efficiency corresponds to maximizing the ratio of output average current with respect to rms switches current, as shown in (19). High primary currents are responsible for most losses during charging.

$$\left\langle I_{out,av}(u)\right\rangle_u / \left\langle I_{p,rms}(u)\right\rangle_u \qquad (19)$$

Ratio (19) is a function of normalized output target voltage k, and therefore solely a function of transformer winding ratio *n*. Taking into account all current values during charging, ratio (19) is averaged in *u* and is exhibited in Figure 9.

Choosing lower *k* enables more efficient charging since the currents ratio is at a higher value, but the trade-off is a higher initial voltage, V_{out0}, enabling resonant charging. Lower *k* corresponds to higher winding ratio and therefore increases $V_{out0}>nV_{in}$. Charging up to V_{out0} is defined as recovery. As resonant charging is not available, other less efficient methods replace it. For example, auto-recovery as explained below. Choosing lower *k* results in reduced recovery efficiency $\eta_{recovery}$, as shown in Figure 9.

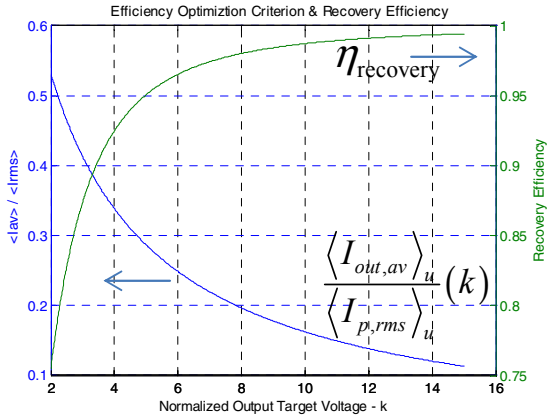

Figure 9: Maximizing efficiency optimization criterion

B. Optimization criterion for reduced dimensions

The transformer is a key part in dictating charger dimensions. Therefore, reducing transformer size helps reduce overall dimensions. A_p is the multiplication of winding area A_w, and core cross-section area A_e as shown in (20). Push-pull transformer winding area compared to one primary winding transformer with the same rms currents results by increased A_w area by 1.205 factor, as shown in appendix A.

$$A_w(k) = \frac{2.41 \cdot n_s \left\langle I_{rms,s}\right\rangle_u}{JK}, \quad A_e(k,\omega) = \frac{\int V_{Lm} dt}{n_p 2B} \qquad (20)$$

Where J [A/m^2] is a winding string cross section rms current, K is the filling winding factor, n_s is secondary winding number, and B[T] is unipolar flax density.

Each transformer core manufacture has its own approximate relation between core density power loss and flax density through switching frequency. Magnetics [12] has the following relations:

$$P_{core} = a f^c B^d \qquad (21)$$

Where P_{core} [mW/cm^3] is the core density power loss, *f* is the switching frequency f_s, and *a,c,d* are approximation constants. Placing A_e expression in Eq (21) we get an expression of core power loss as a function of *u*, which changes during charging. We would like to constrain the average core power loss during complete charging cycle, therefore we would average the expression over *u*:

$$\left\langle P_{core}\right\rangle_u = \frac{10^d a}{\left(2 n_p A_e\right)^d} \cdot \left\langle f_s^c \left(\int V_{Lm} dt\right)^d \right\rangle_u \qquad (22)$$

Rearranging (22), an expression for A_e depending on average charging values, is obtained. Multiplying A_e and A_w expressions results in:

$$A_p(k,\omega) = \frac{12.05 \left\langle I_{rms,p}\right\rangle_u}{JK} \cdot \sqrt[d]{\frac{a}{\left\langle P_{core}\right\rangle_u} \left\langle f_s^c \left(\int V_{Lm} dt\right)^d \right\rangle_u} \qquad (23)$$

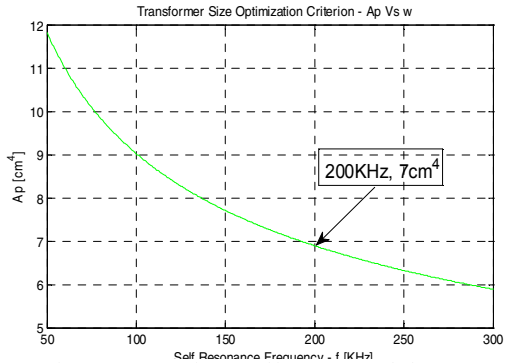

Figure 10: Core size vs self-resonant tank frequency

Where the only expression depending on ω is:

$$\left\langle f_s^c \left(\int V_{Lm} dt \right)^d \right\rangle_u \tag{24}$$

The different dependence of switching frequency and volt-sec effort on ω make it possible for core size reduction. Core size is proportioned to frequency as $A_p \sim 1/\omega^{1-c/d}$. All Magnetics power transformers core materials have c<d therefore 1-c/d>0 and therefore increasing the resonant tank self-frequency decreases core size, while core losses density $\langle P_{core} \rangle_u$ remains unchanged regardless of core size reduction. A_p dependence on ω is exhibited in Figure 10 using prototype charger parameters as shown below.

This behavior should not be strange to us as it was shown that reducing ω, reduces volt-sec effort and therefore smaller core cross-section is needed.

V. Zero Current Switching Active Control

ZCS control contributes to charger high efficiency. The non-conduction period when both switches are off enables partial discharge of resonant capacitor through one of switches parallel built in diodes.

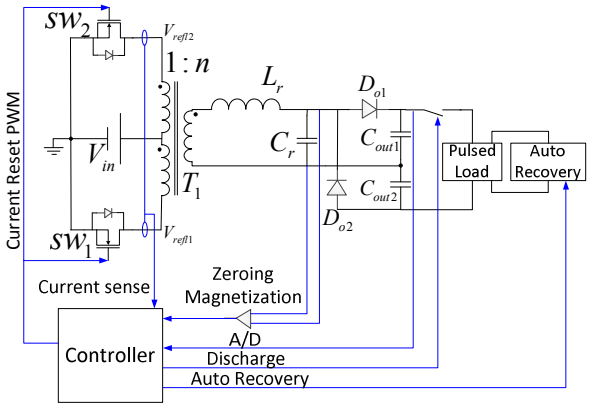

Figure 11: Charger control diagram.

Ignition of a new switching cycle after partial discharge may result in a lack of ability to inject energy to output capacitor, because resonant capacitor will not reach the inverse polarity of output voltage.

One way of solving partial discharge is to place power diodes in series to the switches [13] that would prevent discharge current. Series diodes on high current course would decrease charger efficiency. The present design is avoiding non-conductive periods between switching cycle by the controller. The controller calculates threshold switches current I_{poff} in order to initiate toggle between switches conduction that prevent dead period. Switching of one switch conduction is performed at t_2 while current crosses I_{poff} and conjugate switch turn on is performed at t_4. Conjugated switch is turned on exactly at t_5 while first switch conduction is terminated, creating a short period of time t_5-t_4 that both switches conduct. At first glance, input voltage source is shortened, but deeper examination shows that the input voltage drops on primary leakages, resulting in primary current change of only a few percentages from maximum current.

Switches current is sampled from power stage by a current transformer as shown in Figs. 11, 12.

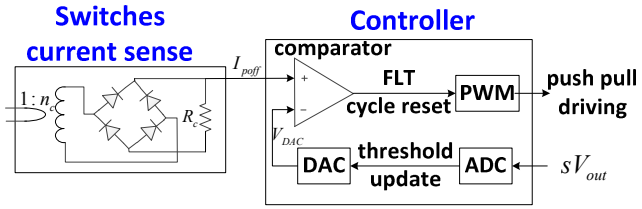

Figure 12: Active ZCS implementation diagram.

One transformer is used to sense both switches current in an opposite direction so that no magnetization reset is needed. Sensed current is fed to the non-inverting input of controller internal analog comparator and compares to internal digital to analog (DAC) calculated reference. DAC reference is calculated by sensing output voltage through an ADC after dividing it by s and feeding it to Eq. (26). Eq. (26), derived from Eq. (25), represents linear discharge of resonant inductance current at linear phase. $I_{poff}(t)=u_c V_{DAC}(t)$ where $u_c=n_c/R_c$ and $sVout(t)=V_{ADC}(t)$.

$$\frac{V_{out}/2 - nV_{in}}{L_r} = \frac{I_{poff}/n}{t_d} \tag{25}$$

$$V_{DAC} = \underbrace{\frac{nt_d s}{2u_c L_r}}_{a} V_{ADC} - \underbrace{\frac{n^2 t_d V_{in}}{u_c L_r}}_{b} \tag{26}$$

Figure 13 exhibits the linear connection, Eq. (26), between V_{DAC}, I_{poff} and output normalized voltage u of prototype charger. Assuming that $T_s \ll t_{ch}$, updating analog comparator reference at least every $5T_s$ ensures approximately non-partial discharge of C_r.

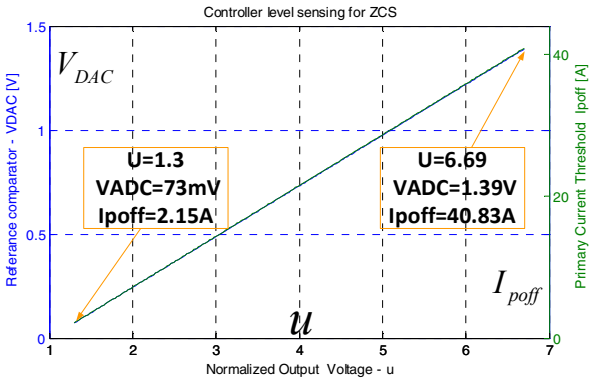

Figure 13: Prototype controller equation. Right plot: Switches current threshold 15A/div; Left plot: DAC reference voltage 0.5V/div.

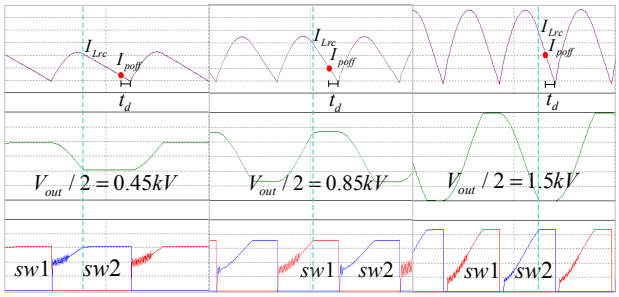

Figure 14: Switching cycles during charging at output voltage of 0.9kV, 1.7kV, 3kV. Top: switches controlled current - 20A/div; Middle: resonant capacitor voltage V_{Cr} - 500V/div; Bottom: reflected switch voltage V_{refl} - 20V/div.

Simulation of three time segments during charging exhibits ZCS varying switching frequency, as shown at Figure 14 The figure shows the varying calculated threshold of switches current (dot), as output voltage increases.

Given the smallest magnetization current under ZCS control, results in asymmetrical magnetization volt-sec effort, as shown in [10]. This positive feedback on magnetization current increases its level during charging. After output capacitor discharge an auxiliary auto recovery circuit, Figure 15, charges output capacitor up to an output level of u=1.3. During this time an oscillation occurs between L_m and C_r due to magnetization current. ZCS charging does not start automatically when u=1.3, it is conditioned by the existence of zero current in L_m. Identification of zero magnetization current is done by locating maximum resonant capacitor voltage by differentially sampling its voltage, as shown in Figure 11.

Auto recovery circuit is controlled by Q_{rc}. Discharging C_{out} initiate recovery process where energy stored in C_{rc} is transferred to output capacitor through D_7,D_5 and R_{rc} (solid arrow). C_{rc} is charged to a normalized voltage u>1.3 in order that after recovery its voltage does not drop below u=1.3. Recovery circuit is buffered from output capacitor and discharge circuit, Q_{dis}, R_{load}, by R_{rc} so that during pulsed load operation C_{rc} would not discharge. During ZCS charging, lost charge is added to recovery capacitor by opening Q_{rc} for conduction (dashed arrow).

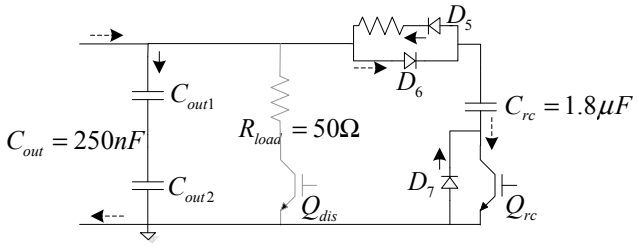

Figure 15: Auto recovery charging circuit. Prototype components values are indicated.

VI. Prototype Charger Measured Results

A prototype charger was implemented to test the feasibility of the proposed topology and its control. Measurements shown in Figure 16 indicate that output voltage increases linearly, as expected, having an approximately constant output current behavior. The output capacitor of 250nF was charged to 3kV in 1.7msec from a low input voltage of 28V. These numbers correspond to an average output power of 0.7kW. The charger was tested periodically at a rate of 586 charging cycles per second. ZCS was maintained through the whole charging process with no gapping between cycles.

Recovery losses were designed to be 3% and therefore according to Figure 9, k=6.7; hence winding ratio is n=8. Charging time requirement, neglecting auto recovery influence, is t_{ch}=860µsec and thus impedance of resonant tank is Z_0=121Ω. Figure 10 indicates that by choosing natural frequency of ω=2π·200kHz, we obtain a transformer core size of A_p=7cm^4. Z_0,ω values result in the following resonant tank components: L_r=100µH,C_r=6.8nF.

After output discharge by pulsed load operation, recovery is performed up to 2·1.3nVin=582V. ZCS charging includes recovery initialization by which recovery capacitor is recharged as seen in Figure 16 at output voltage between 700V to 800V. Switching frequency changes in a domain of [65kHz,200kHz] and switches peak current reach 100A. The average rms current of each switch during charging is $<I_{sw,rms}>_u$=36.6A.

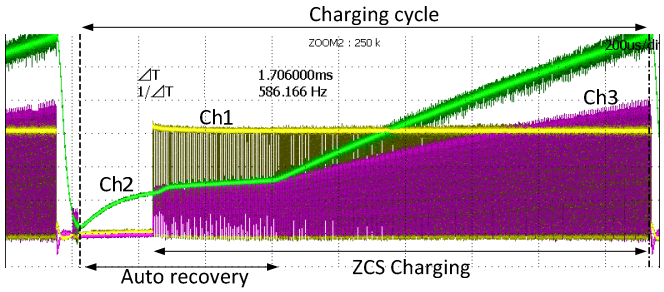

Figure 16: Measured results of the charging cycle. Ch1-controller output - 1V/div; Ch2- output voltage 500V/div; Ch3- switches controlled current - 25A/div; The time scale is 200µsec/div.

Measured efficiency is 84%. Power losses are distributed on the following: 3.2% on switches conduction, 5% on transformer windings conduction, 3% recovery losses and 4.8% on core losses, output diode conduction, input capacitors ESR and conduction in circuit connections.

VII. Conclusion and Future Work

The present study demonstrates the feasibility of a *rapid* high-voltage, high power, push-pull resonant charger based upon self-oscillating parallel topology, which is fed from low input source voltage of 28V. Auto-recovery of the output voltage to a level enabling ZCS charging, as well as zeroing the magnetization DC current at the beginning of each charging cycle, were performed in order to overcome topology weaknesses. During charging process, calculations are continuously performed by the controller to track the varying operation point, so that ZCS is maintained.

The optimization design procedure proposed in this study was verified by simulations and measurements. Two optimization criteria were proposed based on efficiency and core dimensions. Very good agreement was found between the analytical model and experimental results.

Appendix A

Push-pull transformer winding area is:

$$A_{W,\text{push pull}} = \frac{n_p I_{rms,p1}}{JK} + \frac{n_p I_{rms,p2}}{JK} + \frac{n_s I_{rms,s}}{JK} = \frac{\overbrace{\left(\sqrt{2}+1\right)}^{2.41} \cdot n_s I_{rms,s}}{JK} \quad (27)$$

Ratio to transformer with the same rms currents but only one primary is:

$$\frac{A_{W,\text{push pull}}}{A_W} = \frac{2.41}{2} = 1.205 \quad (28)$$

Acknowledgment

The authors would like to thank Rafael Advanced Defense Systems LTD. for funding the research. The technical contribution of Mr. A. Dahan to the prototype charger is highly appreciated.

References

[1] H. Akiyama, T. Sakugawa, T. Namihira, K. Takaki, Y. Minamitani, and N. Shimomura, "Industrial applications of pulsed power technology," in *IEEE Transactions on Industrial Electronics*, vol. 14, no. 5, pp. 1051–1064, Oct. 2007.

[2] R.M. Nelms, B.E. Strickland, and M. Garbi, "High voltage capacitor charging power supplies for repetitive rate loads," in *IEEE 1990 Industry Applications Society Annual Meeting Conference*, 1990, pp. 1281 – 1285.

[3] F. Waag, A. Kuthi, C. Jiang, Q. Zhou, and M. Gundersed, "Flyback resonant charger for high repetition rate pseudospark pulse generator," in *IEEE 2004 power Modulator Symposium*, 2004, pp.85-88.

[4] C. Jourdan, O. Abdel-Rahman, and I. Batarseh, "High-Voltage, High-Power-Density DC-DC Converter for Capacitor Charging Applications," in *IEEE 2009 Applied Power Electronics Conference*, 2009, pp. 433-439.

[5] A.C. Lippincott and R.M. Nelms, "A Capacitor-Charging Power Supply Using a Series-Resonant Topology, Constant On-Time/Variable Frequency Control, and Zero-Current Switching," *IEEE Transactions on Industrial Electronics,* vol. 38, no. 6, pp. 438-447, Dec. 1991.

[6] W. Shen, H. Wang, D. Fu, Y. Pei, X. Yang, F. Wang, D. Boroyevich, F.C. Lee, and C.W. Tipton, "Design and Implementation of High Power Density Three-Level Parallel Resonant Converter for Capacitor Charger" *IEEE Transaction on Plasma Science*, vol 39, no. 4, pp. 1131 – 1140, Apr. 2011.

[7] H. Abe, H. Sakamoto, and K. Harada, "A Noncontact Charger Using a Resonant Converter with Parallel Capacitor of the Secondary Coil," *IEEE Transactions on Industry Applications*, vol 36, no. 2, pp. 444-451, Apr 2000..

[8] A. Pokryvailo, "HIGH POWER, HIGH EFFICIENCY, LOW COST CAPACITOR CHARGER CONCEPT AND DEMONSTRATION," in *IEEE 2009 Pulsed Power Conference*, 2009, pp. 801 - 806.

[9] F.C. Lee, Q. Yang, and F. Wang, "A Novel High-Power-Density Three-Level LCC Resonant Converter With Constant-Power-Factor-Control for Charging Applications," *IEEE Transactions on Power Electronics*, vol. 23, no. 5, pp. 2411-2420, Sept. 2008.

[10] A. Gertsman and S. Ben-Yaakov, "Zeroing transformer's DC current in resonant converters with no series capacitors," in *IEEE 2010 Energy Conversion Congress and Expo*, 2010, pp. 4028-4034.

[11] A. Katz, G. Ivensky, and S. Ben-Yaakov, "Application of Integrated Magnetics in Resonant Converters," in *IEEE 1997 Applied Power Electronics Conference*, 1997, pp. 925-930.

[12] Magnetics 2012 Ferrite Cores Catalog. *www.mag-inc.com.* [Online]

[13] I. Zeltser and S. Ben-Yaakov, "Current Sourcing ZCS Magnetron Driver for Low Input Voltage Applications,"in *IEEE 2011 Applied Power Electronics Conference,* 2011, pp. 877-884.

[14] M.M. Peretz and S.Ben-Yaakov, "A heuristic digital control method for optimal capacitor charging," in *IEEE 2009 Energy Conversion Congress and Exposition*, 2009, pp. 1118-1125.

[15] M.M. Peretz and S.Ben-Yaakov, "A Self-Adjusting Sinusoidal Power Source Suitable for Driving Capacitive Loads," *IEEE Transactions on Power Electronics*, vol 21, no. 4, pp. 890-898, July 2006.